Available online at www.sciencedirect.com

ScienceDirect

Journal of the Franklin Institute 360 (2023) 8918–8935

www.elsevier.com/locate/jfranklin

New power system operational state estimation with cluster of electric vehicles

Hui Gao, Binbin Zang*

College of Automation, College of Artificial Intelligence, Nanjing University of Posts and Telecommunications, NO.9 Wenyuan Road, Yadong Xincheng, Nanjing 210023, China

Received 24 January 2022; received in revised form 17 May 2022; accepted 22 June 2022
Available online 29 June 2022

Abstract

The access of distributed generation (DG) and a large number of electric vehicles (EVs) have changed the operation mode of power system. Its reliability and stability are facing more and more challenges. Therefore, it is very important to accurately estimate the state of the power system. This paper discusses a new power system state estimation method that is based on the shuffled frog leaping pigeon-inspired optimization algorithm (SFL-PIOA). Firstly, establish EV charging load model and distributed generation probability model (including photovoltaic power generation and wind power generation). Then, considering EVs and DG, the state estimation model of the new power system is built. The objective function and constraint conditions are established, and then the improved SFL-PIOA is used to solve the model. Finally, a simulation example is given to compare the improved algorithms (SFL-PIOA) to initial algorithm (PIOA). The results verify the feasibility and effectiveness of the improved method.

1. Introduction

In recent years, the scale of power grid is expanding and the interconnection degree of power grid is improving. An increasing number of DGs and energy storage equipment make the structure and operation mode of power system become more complicated [1]. The access of DGs and EVs [2] and other energy sources has an impact on the stable operation of the

* Corresponding author.
E-mail address: 1221056303@njupt.edu.cn (B. Zang).

https://doi.org/10.1016/j.jfranklin.2022.06.028
0016-0032/

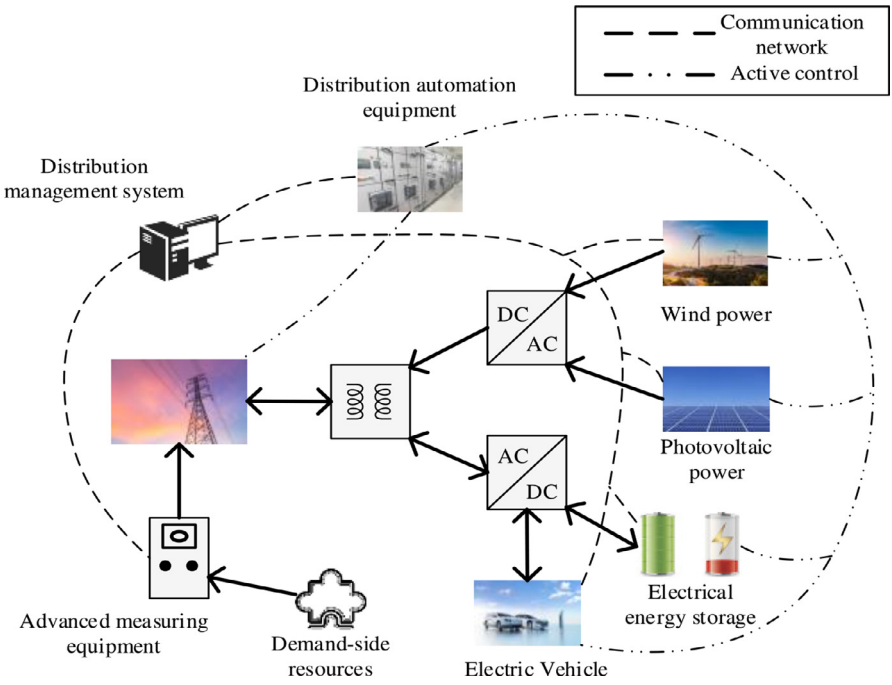

Fig. 1. Composition mode of new power system.

power grid [3,4], while the lack of measurement also interferes with the acquisition of real-time data of the power system, bringing great difficulties to the acquisition of the real-time operation status of the power grid [5]. The state estimation results obtained by the traditional power system state estimation technology can not meet the standard of the whole power system operation scheduling. Therefore, it is of great theoretical significance and practical value to study the state estimation of new power grid.

The research direction of traditional distribution network state estimation is mainly [6]: Reasonable selection of state variables can reduce the sensitivity of state estimation to line parameters [7] and improve the efficiency of state estimation. Commonly used state variables include node voltage, branch current and power [8]; Reasonable optimization of measurement configuration can improve the accuracy and stability of estimation on the premise that the distribution system achieves observability and economy; State estimation methods are reasonably selected. For example, reference [9] applies robust estimation to distribution network, where the system state variable is the square of the amplitude of power and current at the branch head. Literature [10] studies the rational selection of distribution network state estimator and concludes that the weighted least squares (WLS) estimator is reasonably suitable for the distribution network with low measurement redundancy.

With the growth of global demand for energy, more clean energy such as solar energy [11] and wind energy are integrated into the power grid in the form of distributed generation [12], which increases the complexity of the operation mode of the power grid, as shown in Fig. 1. In order to make DG connected to the grid smoothly, on the basis of the above traditional distribution network state estimation technology, the traditional power system will

increase the development of grid access standards such as the location and capacity of the DG, evaluate the safety of the power system, and optimize the control of DG access [5]. However, these measures are based on measurement data with certain errors obtained by system measurement devices, and in practical application, considering the cost and time, there is not enough equipment, coupled with randomness and intermittentness brought by access to DG, will affect the stable operation of power grid control [13]. When EVs are connected to the power grid, they can be used as load when charging and power when discharging, and its charge-discharge characteristics will change the network structure of AC and DC distribution network [14]. EV with the same total output may have different reconstruction results when connected to DC node or AC node, centralized or decentralized [15]. For EVs access with different outputs [16], different network losses and node voltage levels may also affect network reconstruction schemes [17]. When AC/DC power distribution network changes from passive network to active network due to EV access, the power flow distribution of the system changes, and the power flow algorithm of the traditional distribution network and AC/DC power transmission system is no longer applicable [18]. Therefore, the traditional power grid operation management mode can no longer meet the requirements of the stable operation of the power grid [19], and is gradually changing into a new power system with the introduction of multiple types of DG [20]. At present, there are few studies on distribution network state estimation considering distributed power supply and electric vehicle. In order to improve the accuracy of state estimation of new power system, refined smart electricity meter is used to improve the accuracy of network parameters measurement [21]. Some new algorithms are also used to estimate the state of the power system, including newton-Gaussian method based on least squares, semi-positive definite relaxation method and some intelligent algorithms, which improve the accuracy of state estimation to a certain extent [22]. Fast and accurate estimation of the state of the new power system is conducive to DG optimization, reactive voltage control and power grid security assessment [23]. It is important to study the state estimation of the new power system with DG for intelligent distribution system.

This paper contains six sections altogether. In Section 2, the probabilistic model of electric vehicles and the charging power model of cluster electric vehicles are established. Section 3 constructs a probabilistic model for photovoltaic power generation and a probabilistic model for wind power generation. In Section 4, the power system state estimation objective function is constructed, and the pigeon-inspired optimization pigeons algorithm is improved by shuffled frog leaping strategy to form the power system state estimation model. In Section 5, an example is used to verify the method. The last section is the summary of the whole article.

2. Electric vehicle charging load modeling

2.1. Probabilistic model of electric vehicle charging load

The disorder of EV charging load makes it different from conventional load. EV load not only has randomness at a certain time, but also has time variability and volatility at a certain time [24]. The EV charging load model established in this paper assumes that the starting charging time and daily mileage do not interfere with each other, and the user starts charging immediately after returning home from the trip until it is fully charged. Then its Probability

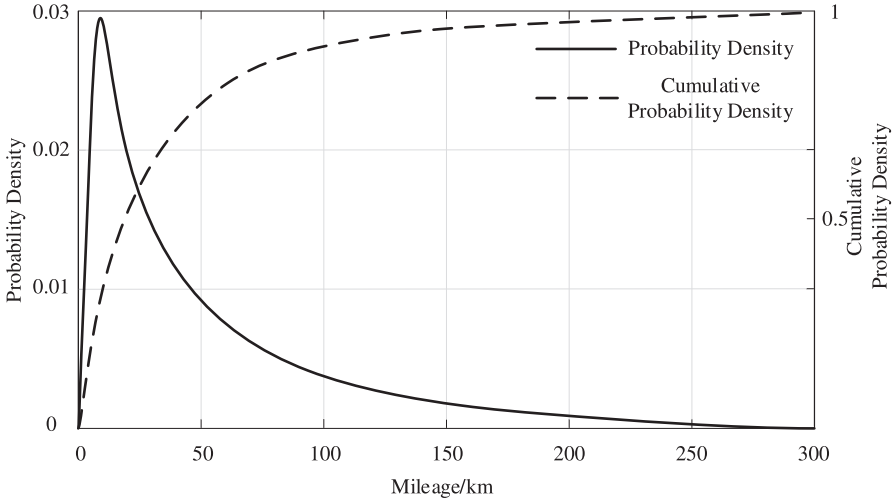

Fig. 2. Probability distribution of daily distance travelled.

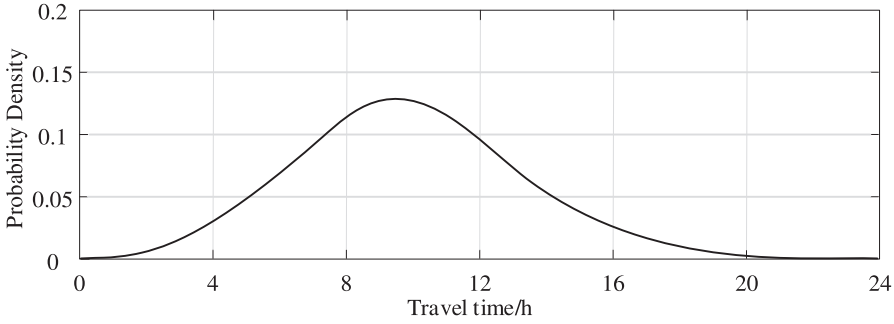

Fig. 3. Probability distribution of travel time.

Density Function is as follows:

$$f(d) = 1/\left(d\sigma_d\sqrt{2\pi}\right) \cdot \exp\left(-(\ln d - \mu_d)^2/2\sigma_d^2\right) \tag{1}$$

Where: d is mileage, set μ_d=3.41, σ_d=1.23. The probability distribution of daily driving distance of electric vehicles is shown in Fig. 2.

The first trip time of electric vehicles is expressed by Eq. (2), and its probability density function is composed of two normal distribution functions. The travel time probability density curve is shown in Fig. 3.

$$f_c(t) = \begin{cases} 1/\left(\sigma_c\sqrt{2\pi}\right) \cdot \exp\left[-(t-\mu_c)^2/\left(2\sigma_c{}^2\right)\right], & 0 < t < \mu_c + 12 \\ 1/\left(\sigma_c\sqrt{2\pi}\right) \cdot \exp\left[-(t-\mu_c)^2/\left(2\sigma_c{}^2\right)\right], & \mu_c + 12 < t < 24 \end{cases} \tag{2}$$

Where: μ_c =8.67, σ_c=3.23.

The probability density function of the return time of the EV is Eq. (3). Finally, the return time probability density curve is shown in Fig. 4. Finally, the return time probability density

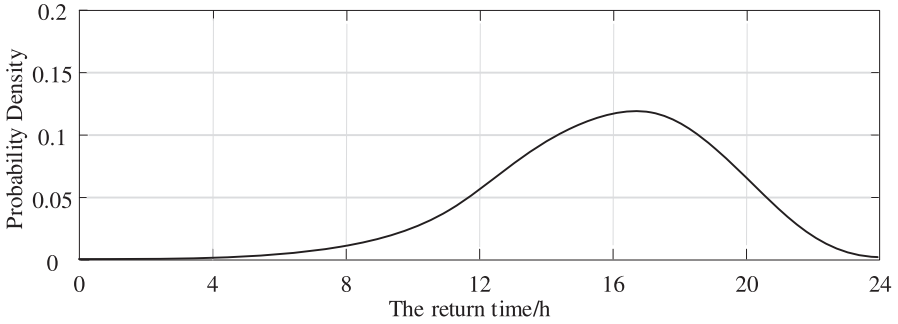

Fig. 4. Probability distribution of return time.

curve is shown in Fig. 4.

$$f_s(t) = \begin{cases} 1/\left(\sigma_s\sqrt{2\pi}\right) \cdot \exp\left[-(t-\mu_s)^2/\left(2\sigma_s^2\right)\right], 0 < t < \mu_s + 12 \\ 1/\left(\sigma_s\sqrt{2\pi}\right) \cdot \exp\left[-(t-24-\mu_s)^2/\left(2\sigma_s^2\right)\right], \mu_s + 12 < t < 24 \end{cases} \tag{3}$$

Where: set μ_s=16.48, σ_s=3.26.

2.2. Charging power model of cluster electric vehicles

The charging power of EV i in time period t is not only related to EV charging start time t_i, but also related to charging duration T_{ic}. In the case of disordered charging, EV is considered to be connected to the power grid immediately after the end of the day's trip, so the moment when EV starts charging is the end of the day's trip. The charging duration Tic of EV i is as follows:

$$T_{\mathrm{ic}} = \min\left((R_i W_i)/(100P_i), T_{i0}\right) \tag{4}$$

Where, R_i represents the daily mileage of electric vehicle i; P_i represents the charging power of electric vehicles; W_i represents the 100 km power consumption of the electric vehicle i; T_{i0} represents the stopping time of electric vehicles, and its value can be expressed by Eq. (5)

$$T_{\mathrm{i0}} = 24 - T_{i,e} + T_{i,s} \tag{5}$$

Where: $T_{i,e}$, $T_{i,s}$, respectively, represent the end time of daily distance of travel and the first trip time of EV i.

The charging power Pi (t) of EV i at time period t is as follows:

$$P_i(t) = \begin{cases} P_i & t_i \le t \le t_i + T_{ic} \\ 0 & else \end{cases} \tag{6}$$

Large-scale cluster EV charging model can be obtained based on EV charging characteristic model and EV driving rule model [25]. To study the charging of a cluster of N electric vehicles, assume that the electric vehicles are connected to the grid for charging immediately after the end of a day's journey. Then the charging power of the electric vehicles connected to the grid at time t during the day is shown as Eq. (7).

$$P(t) = \sum_{i=1}^{N} P_i(t) \tag{7}$$

3. Probabilistic model of distributed generation

3.1. Probabilistic model of photovoltaic generation

Light intensity has randomness and can approximately obey Beta distribution in a period of time [26]. Its probability density function is:

$$f(r) = (\Gamma(\alpha+\beta)/\Gamma(\alpha)\Gamma(\beta)) \cdot (r/r_{\max})^{\alpha-1} \cdot ((r_{\max}-r)/r_{\max})^{\beta-1} \tag{8}$$

Where: the maximum radiation intensity in this period; Γ is the Gamma function. α and β are the parameters of Bate distribution, and their values can be calculated from the mean value μ and standard deviation σ of light intensity during this period, and the values are, respectively:

$$\alpha = \mu\left[(\mu(1-\mu))/\sigma^2 - 1\right] \tag{9}$$

$$\beta = (1-\mu)\left[\mu(1-\mu)/\sigma^2 - 1\right] \tag{10}$$

Where: μ is the mean value under a certain light intensity in this period; σ is the standard deviation at a given light intensity during this period.

Distributed photovoltaic generation consists of a series of solar panels, the number of panels is M. Assume that the area and photoelectric conversion efficiency of each panel are Am and η_m, $m=1,2\ldots, M$, then the active power output P_{PV} of distributed photovoltaic is:

$$P_{PV} = \mathrm{r} \cdot \sum_{m=1}^{M} A_m \cdot \left(\sum_{m=1}^{M} A_m \cdot \eta_m / \sum_{m=1}^{M} A_m \right) \tag{11}$$

According to Eqs. (8) and (11), the probability density function of distributed photovoltaic output can be expressed as:

$$f(P_{PV}) = \Gamma(\alpha+\beta)/\Gamma(\alpha)\Gamma(\beta) \cdot (P_{PV}/R_{\mathrm{m}})^{\alpha-1} \cdot (1 - P_{PV}/R_{\mathrm{m}})^{\beta-1} \tag{12}$$

Where: R_m is the maximum active power output value of distributed photovoltaic. The calculation expression is:

$$R_m = \mathrm{r}_{\max} \cdot \sum_{m=1}^{M} A_m \cdot \left(\sum_{m=1}^{M} A_m \cdot \eta_m / \sum_{m=1}^{M} A_m \right) \tag{13}$$

3.2. Probabilistic model of wind generation

The output of distributed wind power is mainly converted from wind energy to electric energy by wind generators [27], and its output is mainly related to wind speed, which is typically uncertain. The probability density function of wind speed v is:

$$f(v) = \alpha/\beta \cdot (v/\beta)^{\alpha-1} \cdot \exp\left[-(v/\beta)^{\beta}\right] \tag{14}$$

Where, α and β are the shape parameters and scale parameters of the function. The functional relationship between active power output P_W and wind speed v of distributed wind power is as follows:

$$P_W = \begin{cases} 0 & v < v_c \\ k_1 v + k_2 & v_c \le v < v_r \\ P_r & v_r \le v < v_t \\ 0 & v > v_t \end{cases} \tag{15}$$

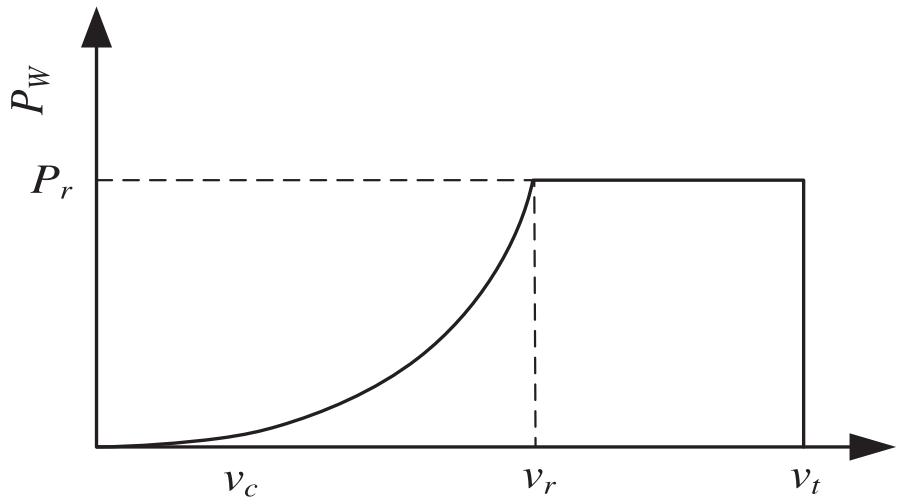

Fig. 5. Power characteristic curve of distributed wind power.

$$k_1 = P_r/(v_r - v_c) \tag{16}$$

$$k_2 = P_r v_c/(v_r - v_c) \tag{17}$$

Where, Pr is the rated power value; Vr, Vc and Vt are the rated wind speed value, cut wind speed and cut wind speed of the fan, respectively. The P_W function curve of distributed wind power output is shown in Fig. 5.

According to Eqs. (14) and (15), the probability density function of distributed wind power output can be expressed as:

$$f(P_W) = \alpha/k_1\beta \cdot ((P_W - k_2)/k_1\beta)^{\alpha-1} \cdot \exp\left[-((P_W - k_2)/k_1\beta)^{\alpha}\right] \tag{18}$$

4. State estimation model of the new power system

4.1. Objective function

In the state estimation of power system, the error of quantity measurement is called measurement error. All measurement errors in the system are given the same weight coefficient, which will lead to the decline of state estimation accuracy [28]. Therefore, the objective function of the weighted least square estimation method is adopted in this paper, and different weight coefficients are given to different precision. The high precision is given high weight, and the low precision is given low weight. The objective is to minimize the sum of squares of the difference between the measured value and the estimated value. The objective function of the state estimation model is:

$$\min J(X) = \sum_{k=1}^{K} \omega_k (z_k - h_k(X))^2 \tag{19}$$

Where, K is the total number of measured nodes; k is the serial number of the measuring node. ω_k is the weight factor of the kth node; z_k is the measured value of the kth node; $h_k(X)$ is the measurement equation of the kth node.

The voltage, active power and reactive power parameters of nodes are taken as state values to be estimated, and the network nodes of power system are divided into DG nodes and load nodes. The active power in power system is divided into DG active power and load active power, and the same reactive power is also divided into DG reactive power and load reactive power. The specific formula is expressed as Eqs. (20)–(23):

$$X_k = [U_k, P_k, Q_k];\ k = 1, 2, \ldots, n \tag{20}$$

$$\begin{cases} P_G = [P_{G1}, P_{G2}, \ldots, P_{Gd}]_{(1*d)} \\ P_L = [P_{L1}, P_{L2}, \ldots, P_{Ld}]_{(1*l)} \end{cases};\quad P_k \in (P_G \cup P_L) \tag{21}$$

$$\begin{cases} Q_G = [Q_{G1}, Q_{G2}, \ldots, Q_{Gd}]_{(1*d)} \\ Q_L = [Q_{L1}, Q_{L2}, \ldots, Q_{Ld}]_{(1*l)} \end{cases};\quad Q_k \in (Q_G \cup Q_L) \tag{22}$$

$$n = d + l \tag{23}$$

Where, X is the state variable; U_k is the node voltage; P_G is the active power of DG; P_L is the active power of load; Q_G is the reactive power of DG; Q_L is reactive power of load; d is the number of DG nodes; l is the number of load nodes; n is the total number of distribution network nodes.

4.2. Constraints

According to the power flow constraint equation of the new power system, the equation constraint conditions of the model objective function are established, which can be expressed as:

$$\begin{cases} P_i = U_i \sum_{j=1}^{n} U_j\left(G_{ij}\cos\delta_{ij} - B_{ij}\sin\delta_{ij}\right) \\ Q_i = U_i \sum_{j=1}^{n} U_j\left(G_{ij}\cos\delta_{ij} + B_{ij}\sin\delta_{ij}\right) \\ (\mathrm{i} = 1, 2, \ldots, n;\ \ j = 1, 2, \ldots, n) \end{cases} \tag{24}$$

Where, i and j are the nodes (including DG node and load node); P_i is the active power of node i; Q_i is the reactive power of node i; U_i is the voltage amplitude of node i; Uj is the voltage amplitude of node j; δ_{ij} is the difference between node i phase Angle and node j phase Angle; Bij is the imaginary part of the element in the admittance matrix.

Constraint condition Eq. (21) can be expressed as:

$$g_k(X) = 0\ \ (r = 1, 2, \ldots, R) \tag{25}$$

Where, r is the serial number of the constraint conditions of the equation; R is the total number of conditions, R is equal to $2r$.

The inequality constraints of the model are upper and lower limits of state variables, which can be expressed as:

$$\begin{cases} P_{Gi\min} \le P_{Gi} \le P_{Gi\max} \\ P_{Li\min} \le P_{Li} \le P_{Li\max} \end{cases} \tag{26}$$

Where, P_{Gi} is the active power of distributed power node i; $P_{Gi\min}$ is the minimum active power of node i. $P_{Gi\max}$ is the maximum active power of the corresponding node i. P_{Gi} is the active power of load node i; $P_{Li\min}$ is the minimum active power of the corresponding load node i. $P_{Li\max}$ is the maximum active power of the corresponding load node i.

Inequality constraint Eq. (26) can be expressed as:

$$f_m(X) \le 0 \quad (e = 1, 2, \ldots, E) \tag{27}$$

Where, e is the number of inequality constraint conditions; E is the total number of inequality conditions, $E=2e$.

4.3. The shuffled frog leaping pigeon-inspired optimization algorithm

4.3.1. Pigeon-inspired optimization algorithm

Pigeon-inspired Optimization Algorithm (PIOA) simulates the homing navigation process of pigeons based on magnetic field, sun and landmarks, and seeks the optimal solution in the solution space by satisfying constraints in the process of solving the Optimization model [29]. The optimization process can be divided into two phases: magnetic field operator and landmark operator phase. In the magnetic field operator phase, the flock is far away from the destination and mainly navigates according to the magnetic field and the altitude of the sun. When the flock is close to the destination and the ground object can be observed, the landmark operator phase is entered, and the specific steps are as follows:

Step 1: Initialization, randomly generate the initial position of each pigeon.

Step 2: Determine the population size and iteration steps, including phase iteration steps of magnetic field operator and phase iteration steps of landmark operator.

Step 3: Magnetic field operator phase. In the initialization phase of this algorithm, the position and direction of flight are determined according to the position of magnetic field and sun. In this model, each pigeon updates its position according to the latest global optimal solution in the current iteration. Through repeated iteration, the number of iterative steps in the magnetic field operator stage is reached, and then go to Step 4.

Step 4: Some pigeons in the doves may have found a destination or a familiar landmark in the field operator phase, so these pigeons can move quickly to the destination, while other pigeons follow them and enter the landmark operator phase. The landmark operator will order the fitness of the current individual, abandon the individual who is low, and use the center of the remaining pigeon as a landmark as a reference direction for flight.

Step 5: Iterate the calculation repeatedly. Output the final power system state estimate when the number of iteration steps in the landmark operator stage is reached.

4.3.2. Introduce shuffled frog leaping algorithm

The Shuffled Frog Leaping Algorithm (SFLA) [30] is introduced to initialize the pigeon flock Algorithm. The steps of SFLA's are as follows: firstly, the system randomly generates m group state variables, sorts them according to their adaptive values and then divides them into p subgroups. Each subgroup is divided into q, in which p and q satisfy the $p{\cdot}q=m$. The system randomly selects the jth group of state variables into a subgroup for re-ordering, as shown in the following formulas:

$$P_j = 2(m+1-j)/[m(m+1)] \quad j = 1, \ldots, m \tag{28}$$

$$D_S = rand \times (X_B - X_W) \tag{29}$$

$$X_{WNew} = X_{WOld} + D_S \quad (-D_{\max} \le D_S \le D_{\max}) \tag{30}$$

Where, P_j represents the probability of the jth group state variable being selected; X_B represents the optimal solution in the subgroup; X_{WNew} represents the worst solution in the subgroup; D_S represents step size; *rand* represents random factors subject to uniform distribution; X_{WOld} represents the value of the status variable before the update; X_{WNew} represents the updated value of the status variable. As long as X_{WNew} is in the feasible region, the algorithm will continuously calculate the adaptive value of its space, and then judge the size of its adaptive value and the corresponding adaptive value of X_{WOld}. If it is less than, the global optimal solution will replace X_B and update X_{WOld}. If the result does not advance further, the value of the randomly generated state variable is selected instead of X_W, and the calculation is continuously updated (the calculation stops at the number of iterations). When the algorithm searches for the whole population, it mixes all state variables and reshuffles the sorted group, and continues to complete the local search until the iteration terminates or the algorithm ends when the conditions are met.

4.3.3. The steps of shuffled frog leaping pigeon-inspired optimization algorithm

Combined with the hybrid hopping Frog algorithm and flock optimization algorithm, the shuffled frog leaping pigeon-inspired optimization algorithm (SFL-PIOA) is used to solve the above power system state estimation model. The specific steps are as follows:

Step 1: The penalty function method is adopted, that is, the penalty term is introduced into the objective function to change the optimization problem of power system state estimation with constraints into an optimization problem without constraints, and then the filling function method can be used to solve it. According to constraint conditions Eqs. (25) and (27) and objective function Eq. (19), the new objective function is defined as:

$$\min \psi(X, z) = J(X) + z\left\{\sum_{k=1}^{K} G\left[g_k(X)\right] + \sum_{\mathrm{m}=1}^{M} F\left[f_m(X)\right]\right\} \tag{31}$$

Where, z is the penalty factor, and a large positive number is generally taken. The function $G[g_k(X)]$ satisfies the following conditions:

$$\begin{cases} G\left[g_k(X)\right] = 0\,, & g_k(X) = 0 \\ G\left[g_k(X)\right] > 0\,, & g_k(X) \neq 0 \end{cases} \tag{32}$$

The function $F[f_m(X)]$ satisfies the following conditions:

$$\begin{cases} F\left[f_m(X)\right] = 0, & f_m(X) = 0 \\ F\left[f_m(X)\right] \neq 0, & f_m(X) > 0 \end{cases} \tag{33}$$

Step 2: Determine the population size, the number of iterative steps and the accuracy of state estimationδ. The number of iterative steps includes the number of iterative steps of magnetic field operator and landmark operator.

Step 3: Randomly generate m groups of state variable $X_h = (x_1, x_2, \ldots, x_n)$ (including node voltage, active power, reactive power, etc.), $h = 1,2,3\ldots, m$. Set the iterative steps of the hybrid hopping frog algorithm, and initialize it with the hybrid hopping frog model.

Step 4: In the stage of magnetic field operator, the solution was continued based on the initialization data obtained by the hybrid jumping frog algorithm. In this phase, each pigeon

updates its position (an estimate of the state variable) based on the most recent global optimal solution in the current iteration. Assuming that the position and speed of the hth pigeon in the flock are X_h (t) and V_h (t), respectively, then:

$$V_h(t) = V_h(t-1)e^{-Wt} + rand\left(X_p - X_h(t-1)\right) \tag{34}$$

$$X_h(t) = X_h(t-1) + V_h(t) \tag{35}$$

Where, W is the magnetic field operator; *rand* is a random number from 0 to 1. X_p is the global optimal position; T is the number of iterations. After repeated iteration, the estimated value of the state is closer and closer to the real value, and the number of iterative steps in the magnetic field operator stage is reached, and then step 5 is carried out.

Step 5: After the above steps, some of the pigeons in the flock may have found the destination or familiar landmarks (partial estimates in a set of states have been obtained) so that the pigeons can move quickly to the destination. It is assumed that $X_c(t)$ is the central position of the flock, and its fitness is $N_p/2$. In each iteration cycle, the landmark operator will sort the fitness of the current individual, discard the individual with low fitness, and take the center position of the remaining pigeons as the landmark as the reference direction of flight. Its expression is:

$$N_p(t) = N_p(t-1)/2 \tag{36}$$

$$X_c(t) = \left[\sum X_h(t) \cdot fit\left(X_h(t)\right)\right] / \sum fit\left(X_h(t)\right) \tag{37}$$

$$X_h(t) = X_h(t-1) + rand \cdot \left(X_c(t) - X_h(t)\right) \tag{38}$$

Where, N_p is the number of half pigeons in each iteration process, that is, the number of pigeons is halved in each iteration process; $fit(X_h(t))$ is the fitness function of pigeon h.

Step 6: Repeated iterative calculation. When the number of iterative steps reaches the landmark operator stage, the final state estimation value of the power system is output. Fig. 6 is the flow chart of SFL-PIOA.

5. Example analysis

In order to verify the algorithm, IEEE30 power distribution system is taken as an example to calculate the state estimation. Fig. 7 shows the improved IEEE30 power distribution system. During calculation, the reference power is 100MVA and the reference voltage is 10 kV. Distributed photovoltaic is connected to nodes 1, 2, and 5, distributed wind power is connected to nodes 8, 11, and 13, and electric vehicle loads are connected to nodes 16, 17, 18, 20, and 30.

The number of individuals is set as $m = 200$, and the total number of iterative steps is 205 generations. Among them, the number of iterations T_0 of the hybrid leapfrog algorithm is 5, the number of iterative steps T_1 of the magnetic field operator is 150 generations, and the number of iterative steps T_2 of the landmark operator is 50 generations. These parameters are substituted into the power system state estimation optimization model, and the voltage amplitude, active power and reactive power of each node are estimated, respectively according to the solution steps proposed in this paper. Then, estimate the active power state value of DG

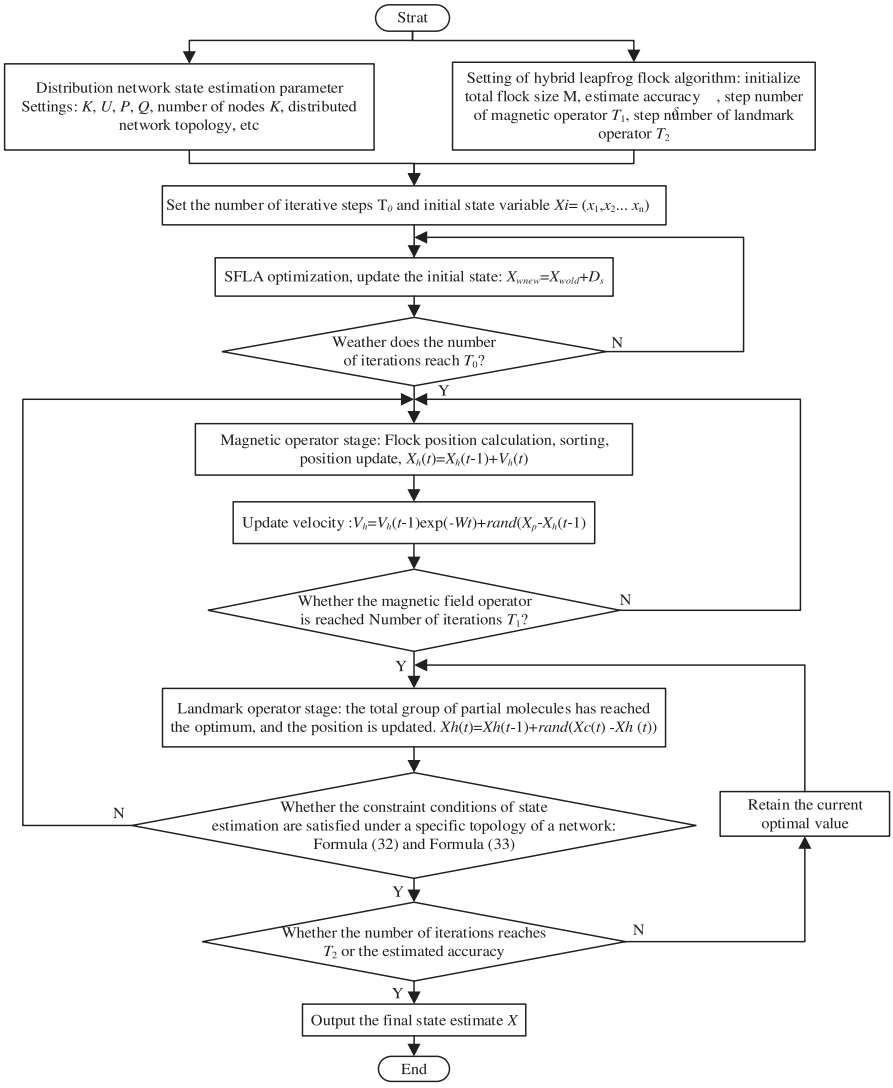

Fig. 6. Flowchart of flock algorithm improved based on mixed leapfrog population division strategy.

connected nodes and the active power state value of each node load. In order to verify the effectiveness of the proposed algorithm, PIOA calculation is used to compare with SFL-PIOA estimation and measurement.

As shown in Figs. 8 and 9, it can be seen that the state estimation results of node voltage amplitude and branch active power using SFL-PIOA are closer to the measured value. However, the estimation results using PIOA, especially the node voltage amplitude state estimation results, are prone to big fluctuations affected by DG and EV access. The result deviation of state estimation is also large. The measured value at node 21 is 1.0235. The improved algorithm reduces the estimated voltage value from 1.035 to 1.0265 and the error rate from 1.12 to 0.29%.

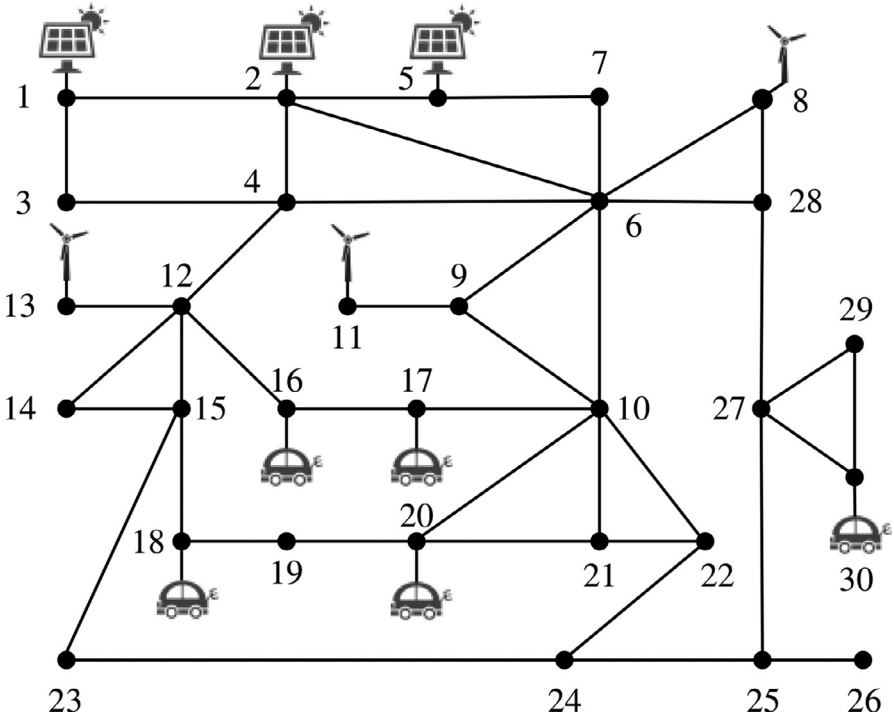

Fig. 7. Wiring diagram of the improved IEEE30 power distribution system.

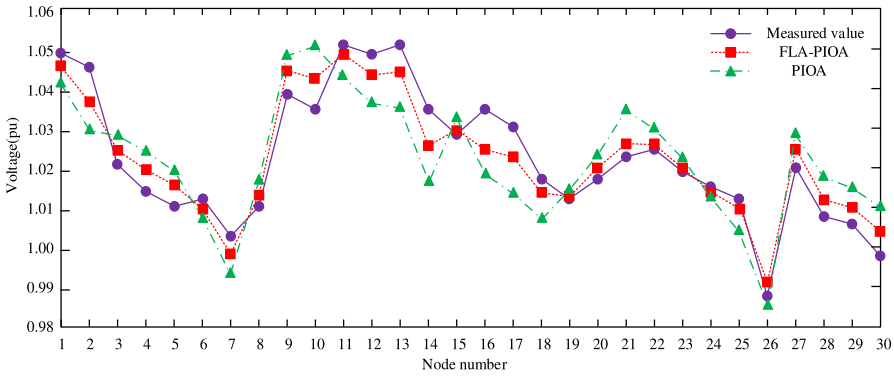

Fig. 8. Node voltage amplitude state estimation result.

As shown in Fig. 10, the state estimation results of reactive power using SFL-PIOA and PIOA branches are very close to the measured values, but the state estimation results of PIOA in branch 36 and branch 38 deviate greatly, especially the branch 36. SFL-PIOA reduced the error from 4.5Kvar to 2Kvar, reducing the error rate by more than 30%.

As shown in Fig. 11, the state estimation results of DG active power of each node using SFL-PIOA and PIOA are compared. It can be seen that the state estimation results of note

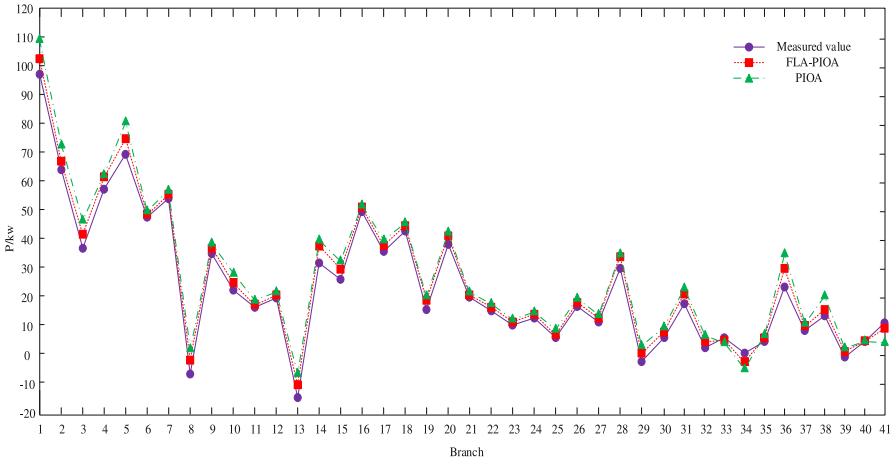

Fig. 9. Estimation results of branch active power state.

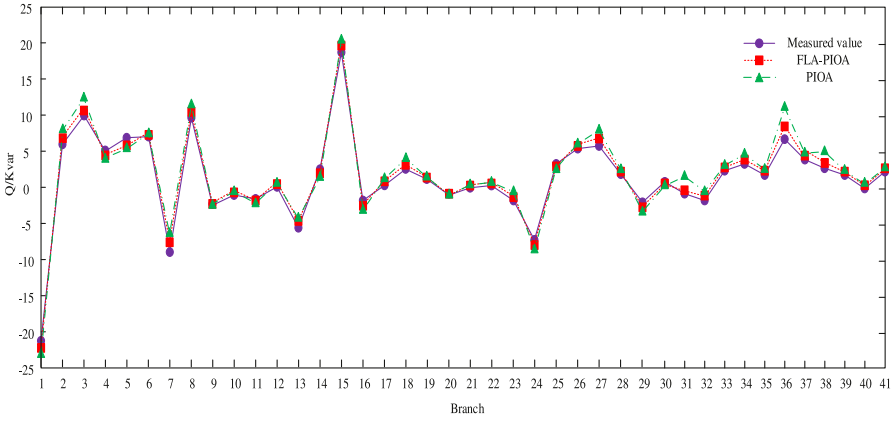

Fig. 10. Estimation results of branch reactive power status.

Table 1
Compares the simulation results of the two algorithms.

Algorithm	First simulation(s)	Second simulation (s)	Third simulation (s)	Fourth simulation (s)
SFL-PIOA	0.0090	0.00108	0.0115	0.0104
PIOA	0.0171	0.0169	0.0182	0.0163

1, node 5 and node 8 using SFL-PIOA are more consistent with the measured values. PIOA has a large deviation at node 5, and the average error of SFL-PIOA is reduced by about 2%.

As shown in Fig. 12, it can be seen that the state estimation results of active power under load of each node under SFL-PIOA are compared with those under PIOA, and it is obvious that the state estimation results under SFL-PIOA are more consistent with the measured values. The average error was reduced by about 4%.

The following is a further analysis and comparison. As shown in Table 1, the calculation time of PIOA algorithm is slightly longer. Compared with PIOA, the speed of solving state

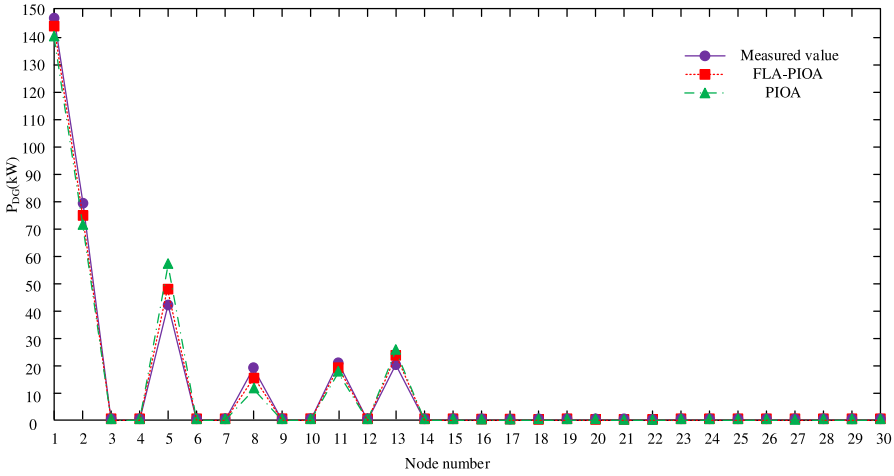

Fig. 11. Comparison of DG active power of each node.

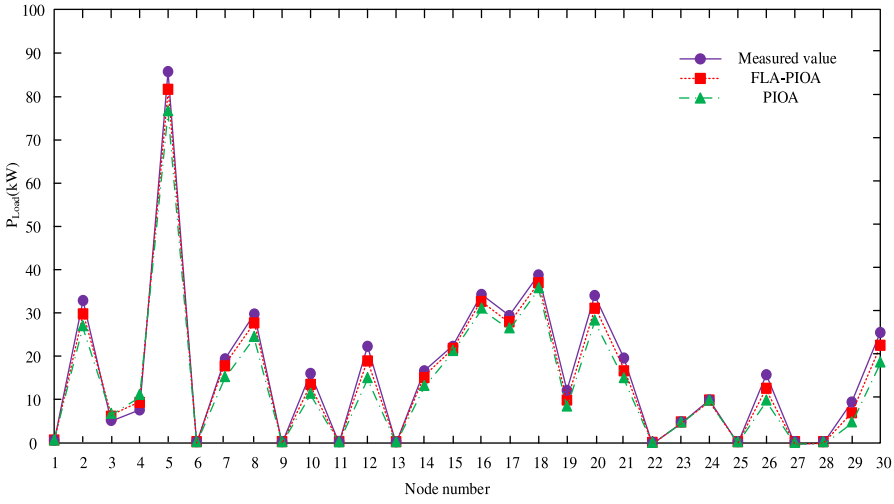

Fig. 12. Comparison of active power of each node load.

estimation parameters using SFL-PIOA is significantly improved. Compared with PIOA, the running time of the improved algorithm is reduced by 39.2% on average.

In order to analyze the state estimation error processing efficiency of SFL-PIOA applied to active distribution network with distributed energy, root mean square error (*RMSE*) and mean absolute error (*MAE*) are defined as follows:

$$RMSE = \sqrt{\frac{1}{P}\sum_{q=1}^{v}(X_E - X_A)^2} \tag{39}$$

$$MAE = \frac{1}{P}\sum_{q=1}^{\mathrm{v}}|X_E - X_A| \tag{40}$$

Table 2
RMES and MAE estimated by SFL-PIOA and PIOA for each state.

Parameter	Algorithm	*RMES*	*MAE*
Node voltage	SFL-PIOA	3.23	2.86
	PIOA	4.72	3.61
Branch active power	SFL-PIOA	3.83	3.46
	PIOA	4.78	4.09
Branch reactive power	SFL-PIOA	2.74	2.15
	PIOA	3.93	3.46
DG active power	SFL-PIOA	3.49	2.74
	PIOA	6.17	5.68
Load active power	SFL-PIOA	2.54	2.31
	PIOA	3.52	2.68

Where, X_E is the estimated value, X_A is the measured value, P is the number of groups, and v is the number of estimated and measured values.

Table 2 shows the data obtained from Fig. 8 to Fig. 12, and then analyzes the *RMSE* and *MAE* comparison of node voltage, line active power, line reactive power, DG active power and load active power, respectively, by SFL-PIOA and PIOA.

As can be seen from the comparison results in Table 2, when SFL-PIOA is used to estimate the state of the power system including distributed energy and electric vehicles, no matter the estimated value of the active power of DG or the active power of the load, The *RMSE* and *MAE* in the estimation results of the improved SFL-PIOA are both smaller than those in the PIOA algorithm. Evaluating overall RMES and MAE, the average values of STL-PIOA were 3.13 and 2.89. The average values of PIOA were 4.52 and 3.86. Compared with the PIOA method, STL-PIOA optimized 30.7 and 25.1%. Therefore, the SFL-PIOA algorithm has a smaller error in calculating the state estimation value, and its algorithm performance is better. Meanwhile, it can be proved that the improved algorithm effectively improves the accuracy of the state estimation of the new power system.

6. Conclusion

In view of the complexity of the new power system and in order to improve the accuracy of state estimation, an improved hybrid pigeon swarm algorithm (SFL-PIOA) is used to estimate the state of the power system containing DG and EVs. The state estimation model of the new power system is established. In order to initialize PIOA population, SFLA was used to improve PIOA, and then SFL-PIOA is used to verify the improved IEEE30 power distribution system. The state estimation values of voltage amplitude, active power and reactive power are compared, and the *RMSE* and *MAE* of the two are compared. The results show that SFL-PIOA is more accurate than PIOA, and has a better state estimation effect. This algorithm can provide a reference for the new power system state estimation method in the future.

Declaration of Competing Interest

We declare that we have no financial and personal relationships with other people or organizations that can inappropriately influence our work, there is no professional or other personal interest of any nature or kind in any product, service and/or company that could be construed as influencing the position presented in, or the review of, the manuscript entitled.

References

[1] A. Ehsan, Q. Yang, Optimal integration and planning of renewable distributed generation in the power distribution networks: a review of analytical techniques, Appl. Energy 210 (2018) 44–59.

[2] T.U. Solanke, V.K. Ramachandaramurthy, J.Y. Yong, J. Pasupuleti, P. Kasinathan, A. Rajagopalan, A review of strategic charging–discharging control of grid-connected electric vehicles, J. Energy Storage 28 (2020) 101193.

[3] A. Ehsan, Q. Yang, State-of-the-art techniques for modelling of uncertainties in active distribution network planning: a review, Appl. Energy 239 (2019) 1509–1523.

[4] H.R. Galiveeti, A.K. Goswami, N.B.D. Choudhury, Impact of plug-in electric vehicles and distributed generation on reliability of distribution systems, Eng. Sci. Technol. 21 (1) (2018) 50–59.

[5] K. Dehghanpour, Z. Wang, J. Wang, Y. Yuan, F. Bu, A survey on state estimation techniques and challenges in smart distribution systems, IEEE Trans. Smart Grid 10 (2) (2018) 2312–2322.

[6] J. Zhao, A. Gómez-Expósito, M. Netto, L. Mili, A. Abur, V. Terzija, et al., Power system dynamic state estimation: motivations, definitions, methodologies, and future work, IEEE Trans. Power Syst. 34 (4) (2019) 3188–3198.

[7] X. Zhang, L. Xu, F. Ding, T. Hayat, Combined state and parameter estimation for a bilinear state space system with moving average noise, J. Frankl. Inst. 355 (6) (2018) 3079–3103.

[8] V. Kekatos, G.B. Giannakis, Distributed robust power system state estimation, IEEE Trans. Power Syst. 28 (2) (2012) 1617–1626.

[9] A.M. Prostejovsky, O. Gehrke, A.M. Kosek, T. Strasser, H.W. Bindner, Distribution line parameter estimation under consideration of measurement tolerances, IEEE Trans. Ind. Inf. 12 (2) (2016) 726–735.

[10] J.K. Watitwa, K.O. Awodele, Active distribution system state estimation: comparison between weighted least squares and extended kalman filter algorithms, in: Proceedings of the IEEE PES/IAS PowerAfrica, IEEE, 2020.

[11] A. Hs, B. An, Optimal design of probabilistically robust PI λ D μ controller to improve small signal stability of PV integrated power system, J. Frankl. Inst. 356 (13) (2019) 7183–7209.

[12] S.M. Ismael, S.H.A. Aleem, A.Y. Abdelaziz, A.F. Zobaa, State-of-the-art of hosting capacity in modern power systems with distributed generation, Renew. Energy 130 (2019) 1002–1020.

[13] L. Zhang, G. Wang, G.B. Giannakis, Real-time power system state estimation and forecasting via deep unrolled neural networks, IEEE Trans. Signal Process. 67 (15) (2019) 4069–4077.

[14] N.O. Kapustin, D.A. Grushevenko, Long-term electric vehicles outlook and their potential impact on electric grid, Energy Policy 137 (2020) 111103.

[15] P. Bastida-Molina, E. Hurtado-Pérez, Á. Pérez-Navarro, D. Alfonso-Solar, P. Research, Light electric vehicle charging strategy for low impact on the grid, Environ. Sci. 28 (15) (2021) 18790–18806.

[16] C. Hou, L. Xu, H. Wang, M. Ouyang, H. Peng, Energy management of plug-in hybrid electric vehicles with unknown trip length, J. Frankl. Inst. 352 (2) (2015) 500–518.

[17] Y. Zhukovskiy, P. Suslikov, N. Russkih, N. Korolev, The use of vehicle-to-grid technology for the integration of electric vehicles in the power system of the city, J.Phys. Conf. Ser. (2019) IOP Publishing.

[18] S. Deb, K. Tammi, K. Kalita, P. Mahanta, Impact of electric vehicle charging station load on distribution network, Energies 11 (1) (2018) 178.

[19] Y.M. Alsmadi, A.M. Abdel-hamed, A.E. Ellissy, A.S. El-Wakeel, A.Y. Abdelaziz, V. Utkin, et al., Optimal configuration and energy management scheme of an isolated micro-grid using Cuckoo search optimization algorithm, J. Frankl. Inst. 356 (8) (2019) 4191–4214.

[20] J. Soares, T. Pinto, F. Lezama, H. Morais, Survey on complex optimization and simulation for the new power systems paradigm, Complex 2018 (2018) 1–32.

[21] A. Al-Wakeel, J. Wu, N. Jenkins, State estimation of medium voltage distribution networks using smart meter measurements, Appl. Energy 184 (2016) 207–218.

[22] A. Primadianto, C.N Lu, A review on distribution system state estimation, IEEE Trans. Power Syst. 32 (5) (2016) 3875–3883.

[23] C. Ren, Y. Xu, A fully data-driven method based on generative adversarial networks for power system dynamic security assessment with missing data, IEEE Trans. Power Syst. 34 (6) (2019) 5044–5052.

[24] K. Chaudhari, N.K. Kandasamy, A. Krishnan, A. Ukil, H.B. Gooi, Agent-based aggregated behavior modeling for electric vehicle charging load, IEEE Trans. Ind. Inf. 15 (2) (2018) 856–868.

[25] H. Liang, Z. Lee, G. Li, A calculation model of charge and discharge capacity of electric vehicle cluster based on trip chain, IEEE Access 8 (2020) 142026–142042.

[26] U.K. Das, K.S. Tey, M. Seyedmahmoudian, S. Mekhilef, M.Y.I. Idris, W. Van Deventer, et al., Forecasting

of photovoltaic power generation and model optimization: a review, Renew. Sustain. Energy Rev. 81 (2018) 912–928.

[27] P. Du, J. Wang, W. Yang, T. Niu, A novel hybrid model for short-term wind power forecasting, Appl. Soft Comput. 80 (2019) 93–106.

[28] Y.M. Ruckstuhl, T. Janjić, Parameter and state estimation with ensemble Kalman filter based algorithms for convective-scale applications, Q. J. R. Meteorol. Soc. 144 (712) (2018) 826–841.

[29] Z. Cui, J. Zhang, Y. Wang, Y. Cao, X. Cai, W. Zhang, et al., A pigeon-inspired optimization algorithm for many-objective optimization problems, Sci. China Inf. Sci. 62 (7) (2019) 1–3.

[30] M. Karakoyun, A. Ozkis, H. Kodaz, A new algorithm based on gray wolf optimizer and shuffled frog leaping algorithm to solve the multi-objective optimization problems, Appl. Soft Comput. 96 (2020) 106560.